



**HAL**  
open science

## Coupling water fluxes with cell wall mechanics in a multicellular model of plant development: Supplementary info for the main article

Ibrahim Cheddadi, Michel Génard, Nadia Bertin, Christophe Godin

### ► To cite this version:

Ibrahim Cheddadi, Michel Génard, Nadia Bertin, Christophe Godin. Coupling water fluxes with cell wall mechanics in a multicellular model of plant development: Supplementary info for the main article. 2019. hal-02788248

**HAL Id: hal-02788248**

**<https://hal.inrae.fr/hal-02788248v1>**

Preprint submitted on 5 Jun 2020

**HAL** is a multi-disciplinary open access archive for the deposit and dissemination of scientific research documents, whether they are published or not. The documents may come from teaching and research institutions in France or abroad, or from public or private research centers.

L'archive ouverte pluridisciplinaire **HAL**, est destinée au dépôt et à la diffusion de documents scientifiques de niveau recherche, publiés ou non, émanant des établissements d'enseignement et de recherche français ou étrangers, des laboratoires publics ou privés.



Distributed under a Creative Commons Attribution - NonCommercial - NoDerivatives 4.0 International License

# Coupling water fluxes with cell wall mechanics in a multicellular model of plant development

Ibrahim Cheddadi<sup>a,b,1</sup>, Michel Génard<sup>c</sup>, Nadia Bertin<sup>c</sup>, and Christophe Godin<sup>b,d,1</sup>

<sup>a</sup>Univ. Grenoble Alpes, CNRS, Grenoble INP, TIMC-IMAG, 38000 Grenoble, France; <sup>b</sup>Virtual Plants, Inria, Montpellier, France; <sup>c</sup>PSH, INRA, Avignon, France; <sup>d</sup>Laboratoire Reproduction et Développement des Plantes, Univ Lyon, ENS de Lyon, UCB Lyon 1, CNRS, INRA, Inria, F-69342, Lyon, France

This manuscript was compiled on January 4, 2019

**The growth of plant organs is a complex process powered by osmosis that attracts water inside the cells; this influx induces simultaneously an elastic extension of the walls and pressure in the cells, called turgor pressure; above a threshold, the walls yield and the cells grow. Based on Lockhart's seminal work, various models of plant morphogenesis have been proposed, either for single cells, or focusing on the wall mechanical properties. However, the synergistic coupling of fluxes and wall mechanics has not yet been fully addressed in a multicellular model. This work lays the foundations of such a model, by simplifying as much as possible each process and putting emphasis on the coupling itself. Its emergent properties are rich and can help to understand plant morphogenesis. In particular, we show that the model can display a new type of lateral inhibitory mechanism that could contribute to the amplification of growth heterogeneities, essential for shape differentiation.**

Plant growth and morphogenesis | Biophysics | Mathematical modelling  
| Emergence | Lateral inhibition

Plants grow throughout their lifetime at the level of small regions containing undifferentiated cells, the meristems, located at the extremities of their axes. Growth is powered by osmosis that tends to attract water inside the cells. The corresponding increase in volume leads to simultaneous tension in the walls and hydrostatic pressure (so-called turgor pressure) in the cells. Continuous growth occurs thanks to the yielding of the walls to these stretching forces [1–3].

This interplay between growth, water fluxes, wall stress and turgor was first modelled by Lockhart in 1965 [4], in the context of a single elongating cell. Recent models focused on how genes regulate growth at more integrated levels [5–9]. To accompany genetic, molecular, and biophysical analyses of growing tissues, various extensions of Lockhart's model to multicellular tissues have been developed. The resulting models are intrinsically complex as they represent collections from tens to thousands of cells in 2- or 3-dimensions interacting with each other. To cut down the complexity, several approaches abstract organ multicellular structures as polygonal networks of 1D visco-elastic springs either in 2D [7, 10–12] or in 3D [6, 13] submitted to a steady turgor pressure. Other approaches try to represent more realistically the structure of the plant walls by 2D deformable wall elements able to respond locally to turgor pressure by anisotropic growth [8, 14, 15].

Most of these approaches consider turgor as a constant driving force for growth, explicitly or implicitly assuming that fluxes occur much faster than wall synthesis. Cells then regulate the tissue deformations by locally modulating the material structure of their walls (stiffness and anisotropy) [6, 16–20]. However, the situation in real plants is more complex: turgor heterogeneity has been observed at cellular level [21, 22], which challenges the assumption of very fast

fluxes. As a matter of fact, the relative importance of fluxes or wall mechanics as limiting factors to growth has fuelled a long standing debate [3, 23] and is still an open question. Moreover, from a physical point of view, pressure is a dynamic quantity that permanently adjusts to both mechanical and hydraulic constraints, which implies that a consistent representation of turgor requires to model both wall mechanics and hydraulic fluxes.

The aim of this article is to explore the potential effect of coupling mechanical and hydraulic processes on the properties of the "living material" that corresponds to multicellular populations of plant cells. To this end, we build a model that describes in a simple manner wall mechanics and cell structure, but do not compromise on the inherent complexity of considering a collection of deformable object hydraulically and mechanically connected.

The article is organized as follows (see Fig. 1): we first recall the Lockhart-Ortega model and its main properties. Then we explore two simple extensions of this model: first we relax the constraint of uniaxial growth in the case of a single polygonal cell; then we study how two cells hydraulically connected interact with each other. Finally we describe our multicellular and multidimensional model and numerically explore its properties.

## Significance Statement

Plant cells are surrounded by a rigid wall that prevents cell displacements and rearrangements as in animal tissues. Therefore, plant morphogenesis relies only on cell divisions, shape changes, and local modulation of growth rate. It has long been recognized that cell growth relies on the competition between osmosis that tends to attract water into the cells and wall mechanics that resists to it, but this interplay has never been fully explored in a multicellular model. The goal of this work is to analyze the theoretical consequences of this coupling. We show that the emergent behavior is rich and complex: among other findings, pressure and growth rate heterogeneities are predicted without any ad-hoc assumption; furthermore the model can display a new type of lateral inhibition based on fluxes that could complement and strengthen the efficiency of already known mechanisms.

This study was initiated by C.G., M.G., and N.B. I.C. designed the model with the help of C.G. and M.G. performed the mathematical calculations with the help of C.G., designed the resolution algorithm, implemented it, ran simulations, and explored the parameters space. I.C. and C.G. analyzed the results and wrote the manuscript with inputs from other authors.

The authors declare no conflict of interest.

<sup>1</sup>To whom correspondence should be addressed. E-mail: [ibrahim.cheddadi@univ-grenoble-alpes.fr](mailto:ibrahim.cheddadi@univ-grenoble-alpes.fr), [christophe.godin@inria.fr](mailto:christophe.godin@inria.fr)

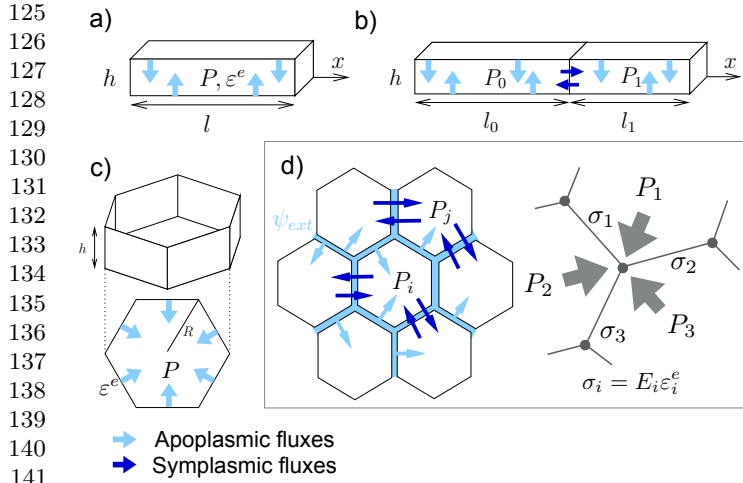


**Fig. 1.** Hierarchy of models presented in this article. Main variables are turgor  $P$  and elastic deformation  $\varepsilon^e$ . **a)** Lockhart-Ortega model: uniaxial growth in the  $x$  direction of a cylindrical cell of length  $l$ ; the section perpendicular to  $x$  is a square of side  $h$ . **b)** Two cells extension, both growing along  $x$ ; **c)** 2D extension of a single cell growth; **d)** Multicellular, multidimensional model; left: fluxes, right: mechanical equilibrium; the stress  $\sigma$  is proportional to the elastic deformation  $\varepsilon^e$ ;  $E$  is the elastic modulus.

## The Lockhart model

In 1965, Lockhart [4] derived the elongation of a cylindrical plant cell by coupling osmosis-based fluxes and visco-plastic wall mechanics. Ortega [24] extended this seminal model to include the elastics properties of the cell walls. We recall here the main properties of this model, see Fig. 1a for the geometrical configuration.

**Cell wall elongation.** It is expressed as a rheological law [4, 24]: the total strain rate of the walls  $\dot{\varepsilon}$  is decomposed into the sum of a plastic and an elastic strain rate:

$$\dot{\varepsilon} = \phi^w (P - P^Y)_+ + \frac{1}{\bar{E}} \frac{dP}{dt}, \quad [1]$$

where the extensibility  $\phi^w$  (inverse of a viscosity) describes the ability of the cell to synthesize wall material, and  $\bar{E}$  is an effective elastic modulus. Here,  $\phi^w$  and  $\bar{E}$  both depend on cell wall thickness. The notation  $(x)_+$  denotes  $x$  if  $x > 0$  and 0 otherwise for any real number  $x$ .

**Water uptake.** Lockhart described water uptake by the cell as a flux through a semi-permeable membrane characterized by its surface  $A$  and its permeability  $L^a$ . Assuming the membrane is perfectly impermeable to solutes, the rate of volume change is the result of a difference between the water potential  $\Psi$  of the cell and  $\Psi_{ext}$  of its exterior [25]:

$$\frac{dV}{dt} = AL^a (\Psi_{ext} - \Psi), \quad [2]$$

The cell water potential  $\Psi = P - \pi$  results from the antagonistic effect of the cell hydrostatic pressure  $P$  that tends to expel water from the cell and its osmotic pressure  $\pi$  that tends to attract water inside the cell. In the case of a single solute of concentration  $c$ , we have  $\pi = RTc$  where  $R$  is the ideal gas constant and  $T$  the temperature. Let us denote  $\phi^a = \frac{AL^a}{V}$  which has the same dimension as  $\phi^w$ . Assuming that the fluxes occur mostly on the lateral surface, the ratio  $A/V$  is constant

in the configuration of a cylindrical cell. After division by  $V$ , Eq. (2) turns into:

$$\dot{\gamma} = \phi^a (P^M - P), \quad [3]$$

where  $P^M = \Psi_{ext} + \pi$  quantifies the power of the osmotic pump: it is positive if  $\pi$  is high enough to overcome the negative water potential of the exterior of the cell. Growth ( $\dot{\gamma} > 0$ ) implies  $P < P^M$  and hence  $P^M$  is an upper bound for turgor, above which the cell would lose water to the exterior. The additional condition for growth  $P > P^Y$  (see above) requires  $P^M > P^Y$ : growth is possible only when the osmotic pump is able to overcome the mechanical resistance of the walls.

In order to keep the analysis as simple as possible, we take here and in the remaining of the article  $P^M$  constant with time and homogeneous among the cells, which corresponds for instance to constant  $\pi$  and  $\Psi_{ext}$ . This choice will be commented in the discussion section.

**Coupling hydraulics and mechanics for a single cell.** Equating the expressions of strain rate  $\dot{\varepsilon}$  from Eq. (1) and relative growth rate  $\dot{\gamma}$  from Eq. (3) ensures that the requirements for water uptake and yield of the cell wall are simultaneously satisfied. This means that turgor  $P$ , that is present in both equations, has to be adjusted to satisfy both hydraulic and mechanical constraints. The resolution of the model is detailed in Supplementary Information (SI), Eqs. (S3)-(S4). The time dependent solutions can be analytically determined and we find that  $P$  and  $\dot{\gamma}$  converge towards a stationary solution ( $P^*$ ,  $\dot{\gamma}^*$ ): first,  $P^*$  writes

$$P^* = \alpha^a P^M + (1 - \alpha^a) P^Y, \quad [4]$$

where

$$\alpha^a = \frac{\phi^a}{\phi^a + \phi^w} \in [0, 1] \quad [5]$$

measures the relative importance of  $\phi^a$  compared to  $\phi^w$ . In the limit  $\phi^a \ll \phi^w$  ( $\alpha^a = 0$ ), any excess of turgor above the threshold is relaxed by cell wall synthesis and turgor is minimal at  $P = P^Y$ . Conversely, in the limit  $\phi^w \ll \phi^a$  ( $\alpha^a = 1$ ), the wall synthesis is not able to relax turgor, which reaches then its maximal value  $P = P^M$ . Second, the expression of the relative growth rate is:

$$\dot{\gamma}^* = \frac{\phi^a \phi^w}{\phi^a + \phi^w} (P^M - P^Y), \quad [6]$$

or equivalently:  $P^M - P^Y = \left(\frac{1}{\phi^a} + \frac{1}{\phi^w}\right) \dot{\gamma}^*$ . This equation is the analog of Ohm's law  $\Delta U = (R_1 + R_2)I$  with two resistors  $R_1 = 1/\phi^a$  and  $R_2 = 1/\phi^w$  in series: growth can be limited by either hydraulic conductivity or wall synthesis.

**Link with wall rheology.** Wall expansion law (Eq. (1)) can be equivalently described as a function of wall stress  $\sigma$  rather than cell turgor  $P$ : in the cylindrical geometry of the Lockhart-Ortega model, we find (see SI for the calculations)  $P = \frac{2w}{h}\sigma$ , where  $w$  is the width of the walls and  $h$  their height. Thanks to this relation, Eq. (1) translates into  $\dot{\varepsilon} = \frac{1}{\bar{E}} \frac{d\sigma}{dt} + \Phi^w (\sigma - \sigma^Y)_+$ , where  $E = \frac{h}{2w} \bar{E}$  (resp.  $\Phi^w = \frac{2w}{h} \phi^w$ ) is the intrinsic elastic modulus (resp. extensibility) of the walls. Let  $\varepsilon^e = \sigma/E$  be the so-called elastic deformation of the walls. It is dimensionless and can be measured from the image analysis

249 of experiments, without the knowledge of the elastic modulus.  
250 The wall rheology is then described as follows:

$$251 \quad \dot{\varepsilon} = \frac{d\varepsilon^e}{dt} + \Phi^w E(\varepsilon^e - \varepsilon^Y)_+, \quad [7]$$

252 where  $\varepsilon^Y = \sigma^Y/E$  is the threshold elastic deformation. Note  
253 that  $\frac{1}{\Phi^w E}$  can be interpreted as the characteristic time of wall  
254 synthesis.

## 255 Multidimensional and multicellular models

256 A multicellular extension of the Lockhart-Ortega model  
257 adapted to the study of morphogenesis requires first to relax  
258 the constraint of uniaxial growth and allow multidimensional  
259 geometries, and second is complexified by the possibility of  
260 fluxes between cells. We study separately the effect of each of  
261 these extensions before presenting the complete model.

262 **First extension: Multidimensional growth.** In order to keep the  
263 analysis as simple as possible, we study here the expansion  
264 of a single 2D cell whose shape is a regular polygon with  $n$   
265 edges (see Fig. 1c). This model allows to evaluate the effect  
266 of a varying surface/volume ratio compared to the Lockhart-  
267 Ortega model where this ratio is constant. The fluxes are  
268 described in the same way as for Lockhart's model (Eq. (2))  
269 but wall synthesis is described with Eq. (7), as a function  
270 of elastic deformation instead of turgor. We find (see SI for  
271 detailed calculations) that the relation between cell turgor and  
272 wall stress becomes  $P = \frac{w}{R \cos(\pi/n)} \sigma$  where  $R$  is the cell radius.  
273 In contrast with the Lockhart-Ortega model, the ratio  $P/\sigma$  is  
274 no more constant as cell grows, and the turgor vanishes at long  
275 times if the stress remains in the order of magnitude of the  
276 threshold. Note also that for a given stress the turgor decreases  
277 with the number of edges  $n$ . Therefore, the yield turgor  $P^Y$   
278 depends both on  $n$  and  $R$  and is not a well defined parameter.  
279 It suggests also that cells with less neighbours should have a  
280 higher turgor, as experimentally observed in [21, 22].

281 The prediction of growth rate requires a numerical reso-  
282 lution of the model (see SI). The parameters are chosen to  
283 ensure a turgor of the order of 0.5 MPa and a relative growth  
284 rate of the order of 2% per hour, using the predictions Eq. (4)  
285 and Eq. (6). First let's examine the case of a cell of initial  
286 radius  $R = 10\mu\text{m}$  for which wall synthesis is the limiting factor  
287 to growth (case  $\alpha^a = 0.9$  in SI, fig. S2). We find that it results  
288 initially in an accelerating growth (the bigger the cell, the  
289 faster the growth), much faster than predicted by the Lock-  
290 hart model, during which the elastic deformation of the walls  
291 can reach values up to 20%. The ratio area/surface =  $1/R$   
292 decreases with growth and there is less and less water available  
293 compared to the volume; as a consequence, the relative growth  
294 rate vanishes at long times after this initial accelerating phase.

295 In the case where the fluxes are already limiting in the initial  
296 state (case  $\alpha^a = 0.1$  in SI, Fig. S2), the initial behaviour is  
297 closer to the predictions of the Lockhart model but the relative  
298 growth rate still vanishes at long times.

299 Altogether, these results show that a non constant sur-  
300 face/volume ratio deeply modifies the behavior of the model  
301 compared to the Lockhart model. In particular, flux and wall  
302 synthesis as limiting factors for growth are no more equivalent.

303 **Second extension: Multicellular growth.** Then, we study a sim-  
304 ple multicellular extension of the Lockhart-Ortega model where

311 two cylindrical cells  $i = 0, 1$  are in contact through one of their  
312 wall (see Fig. 1b). The cells can absorb water from their lateral  
313 surface and in the meantime exchange water with each other  
314 through their common wall. We look for stationary solutions:  
315  $\frac{dP_i}{dt} = 0$  and  $\frac{1}{V_i} \frac{dV_i}{dt} = \text{Cst}$ .

316 We set for both cells a common value of  $P^M$ ,  $L^a$  and  
317  $\phi^w$ , while the value of the yield turgors  $P_i^Y$  can differ; this  
318 corresponds for instance to a heterogeneity of wall elastic  
319 modulus or yield deformation. For the sake of convenience, we  
320 refer to fluxes between cells as symplasmic fluxes, characterized  
321 by a water conductivity  $L^s$ , and to fluxes from the water source  
322 as apoplasmic fluxes, characterized by a water conductivity  
323  $L^a$ . Assuming that the symplasmic fluxes occur through  
324 plasmodesmata that are permeable to both water and solutes,  
325 the flux equation writes

$$326 \quad \frac{dV_i}{dt} = A_i L_i^a (P^M - P_i) + A_{01} L^s (P_j - P_i),$$

327 where  $j = 1 - i$ , and  $A_{01}$  is the surface of the common wall  
328 of cells 0 and 1. We introduce the number  $\phi^s = 2A_{01}L^s/V_i$   
329 which has the same dimension as  $\phi^a$  and  $\phi^w$ . In order to allow  
330 an analytical resolution of this set of equations, we assume  $\phi^s$   
331 to be constant with time, and consider it in this section as a  
332 parameter of the model. Thus, we have

$$333 \quad \dot{\gamma}_i = \phi^a (P^M - P_i) + \frac{\phi^s}{2} (P_j - P_i). \quad [8]$$

334 We introduce the dimensionless number

$$335 \quad \alpha^s = \frac{\phi^s}{\phi^s + \phi^a} \in [0, 1]$$

336 which represents the relative importance of symplasmic fluxes  
337 with respect to apoplasmic ones. We combine this flux equation  
338 with the growth equation Eq. (1) and find analytical solutions  
339 for any values of the parameters (see SI). We use here the  
340 following set of control parameters:

$$341 \quad P^M, P_i^Y, \dot{\gamma}_0^*, \alpha^a, \alpha^s,$$

342 and fix the value  $\dot{\gamma}_0^* = 2\% \cdot \text{h}^{-1}$ ; this way, the parameters  
343 space to explore is reduced to  $(P^M, P_i^Y, \alpha^a, \alpha^s)$ . When  $\alpha^s = 0$ ,  
344 the cells are completely isolated one from another and reach  
345 turgors  $P_i^*$  and growth rates  $\dot{\gamma}_i^*$  as predicted by the Lockhart  
346 model (Eq. (4) and Eq. (6)). In particular, the condition  
347  $P^M > P_i^Y$  ensures that each cell is growing. When  $\alpha^s > 0$ ,  
348 the fluxes between cells modify this behaviour. We restrict  
349 to the case  $P_0^Y < P_1^Y < P^M$ , which corresponds to less  
350 mechanical constraints on cell 0 than cell 1; therefore we can  
351 expect  $P_1 > P_0$  and  $\dot{\gamma}_1 < \dot{\gamma}_0$ . The calculations show a complex  
352 non linear behaviour that is illustrated in Fig. 2, in which  
353 the parameters subspace  $(\alpha^a, \alpha^s)$  is explored for given values  
354 of  $P_i^Y$  and  $P^M$  (detailed calculations are provided in SI). Let  
355  $\Delta P^Y = P_1^Y - P_0^Y > 0$  be the difference of the two yield turgors  
356 and  $\bar{P}^Y = 0.5(P_0^Y + P_1^Y)$  their average; we also introduce the  
357 dimensionless number

$$358 \quad \rho = \frac{\Delta P^Y}{2(P^M - \bar{P}^Y)}. \quad [9]$$

359 Note that the hypothesis  $P_0^Y < P_1^Y < P^M$  is equivalent to  
360  $\rho \in ]0, 1[$ .

361 We find that the subspace  $(\alpha^a, \alpha^s)$  can be divided in two  
362 main regions separated by the curve  $\alpha^s = \frac{1-\rho}{1-\alpha^a}$  (see Fig. 2a):

373 surprisingly, in the region  $\alpha^s > \frac{1-\rho}{1-\alpha^a}$ , only cell 0 is growing  
 374 ( $\dot{\gamma}_0 > 0$ ,  $\dot{\gamma}_1 = 0$ , and equivalently  $P_0 > P_0^Y$ ,  $P_1 < P_1^Y$ ). Hence,  
 375 the growth of cell 1 is inhibited by fluxes with cell 0. Conversely,  
 376 in the region  $\alpha^s < \frac{1-\rho}{1-\alpha^a}$  both cells are growing ( $\dot{\gamma}_i > 0$  and  
 377 equivalently  $P_i > P_i^Y$ ). The size of the region  $\alpha^s > \frac{1-\rho}{1-\alpha^a}$   
 378 increases with  $\rho$  and fills the whole square  $[0, 1] \times [0, 1]$  when  
 379  $\rho \rightarrow 1$ ; such values can be reached when  $\Delta P^Y$  is large and /  
 380 or  $P^M$  is close to  $\bar{P}^Y$ .

381 More quantitatively, Figs. 2d-e) show that  $\dot{\gamma}_1$  is always  
 382 below  $\dot{\gamma}_1^*$ , while  $\dot{\gamma}_0$  is always above  $\dot{\gamma}_0^*$  and can reach up to  
 383 twice this value. Furthermore, maximal values of  $\dot{\gamma}_0$  coincide  
 384 with minimal values of  $\dot{\gamma}_1$ : this confirms quantitatively that  
 385 the growth of the cell with less favorable mechanical condition  
 386 is slowed down if not inhibited by the growth of its neighbour.  
 387 This shows also that the growth rate heterogeneity is amplified  
 388 by fluxes.

389 Turgor heterogeneity is also affected by fluxes (see Figs. 2b-  
 390 c): when  $\alpha^s$  is close to zero, the cells are hydraulically isolated  
 391 and their turgors vary with  $\alpha^a$  as predicted by Lockhart model  
 392 (Eq. (4)), this is where the turgor heterogeneity is maximal.  
 393 Conversely, when  $\alpha^s$  is close to 1, there is no hydraulic resis-  
 394 tance between the two cells and the two turgors are equal.  
 395 Between these two limits,  $P_0$  is only slightly affected and re-  
 396 mains in the  $[P_0^Y, P^M]$  interval; conversely,  $P_1$  is dramatically  
 397 affected as it shifts from the interval  $[P_1^Y, P^M]$  when  $\alpha^s = 0$  to  
 398 the interval  $[P_0^Y, P^M]$  when  $\alpha^s = 1$ . Therefore, as  $P_0^Y < P_1^Y$ ,  
 399 there is a region where  $P_1 < P_1^Y$  which corresponds to the  
 400 region  $\alpha^s > \frac{1-\rho}{1-\alpha^a}$ , where cell 1 is not growing.

401 Finally, we have seen that intercellular fluxes tend to in-  
 402 crease (resp. decrease) growth rate (resp. turgor) hetero-  
 403 geneities; the cell with less mechanical constraints takes con-  
 404 trol over the other one and imposes its turgor, which can lead  
 405 the other one to stop growing. The growing cell then benefits  
 406 from the water resources of the other cell and its growth is all  
 407 the more increased.

409 **Generalization: a multidimensional and multicellular model**  
 410 **of growth.** We consider (see Fig. 1d) a collection of  $N$  cells  
 411 that form a (non necessarily regular) 2D mesh with a fixed  
 412 topology (distribution of neighbours) as is the case with plant  
 413 tissues when no division occurs.

414 The cell walls rheology is described by the visco-elasto-  
 415 plastic law (Eq. (7)) of the Ortega model and the fluxes toward  
 416 a cell  $i$  are described as in the simple multicellular model  
 417 presented above:

$$418 \frac{dV_i}{dt} = A_i L_i^a (P^M - P_i) + \sum_{j \in n(i)} A_{ij} L_{ij}^s (P_j - P_i), \quad [10]$$

419 where  $n(i)$  is the set of neighbours of cell  $i$ ,  $A_{ij}$  is the area  
 420 of the common wall with cell  $j$ ,  $L_{ij}^s$  its permeability (it is  
 421 symmetric:  $L_{ij}^s = L_{ji}^s$ ), and  $L_i^a$  is the permeability of the  
 422 lateral walls to the supply of water.

423 The last missing part to obtain a closed set of equation is  
 424 the mechanical equilibrium, that allows to link cells turgors,  
 425 walls tensions, and geometry. Contrary to the cases studied  
 426 above, no explicit expression of turgors as a function of stresses  
 427 can be obtained and the equilibrium has to be solved at each  
 428 time step. Let  $P_i$  be the turgor pressure in each cell  $i$ . The  
 429 tissue being at every moment in a quasi-static equilibrium,  
 430 pressure forces on wall edges and elastic forces within walls

balance exactly at each vertex  $v$ :

$$431 \frac{1}{2} \sum_{k \in f(v)} \Delta_k P S_k \mathbf{n}_k + \sum_{k \in f(v)} E_k \varepsilon_k^e s_k \mathbf{e}_{k,v} = 0, \quad [11]$$

432 where  $f(v)$  is the set of faces adjacent to junction  $v$ ,  
 433  $\Delta_k P = P_{k_1} - P_{k_2}$  is the pressure jump across face  $k$ , with  
 434  $k_1 < k_2$  being indices of the cells across face  $k$ ,  $S_k = h l_k$  is  
 435 the area of the face  $k$  on which pressure is exerted,  $\mathbf{n}_k$  is the  
 436 normal vector to face  $k$ , oriented from cell  $k_1$  to cell  $k_2$ , and  
 437  $s_k = h w$  is the cross-section area of the face, on which the  
 438 elastic stress is exerted; finally,  $\mathbf{e}_{k,v}$  is the unit vector in the  
 439 direction of face  $k$ , oriented from junction  $v$  to the other end  
 440 of face  $k$ .

441 **Coupling mechanical and hydraulic models.** In the Lockhart-  
 442 Ortega model, the compatibility between wall enlargement  
 443 and cell volume variation is automatically enforced through  
 444 the geometrical constraint of uni-directional growth that leads  
 445 to the identity between the relative growth rate of the cell and  
 446 the strain rate of the walls. In contrast, in the multicellular  
 447 model, this identity is no longer true. One has to solve the  
 448 closed set of equations Eq. (7)-Eq. (10)-Eq. (11) with respect  
 449 to the unknowns  $X$ ,  $P$ , and  $\varepsilon^e$ .

450 Despite its apparent simplicity, the problem to be solved  
 451 is not straightforward as water fluxes induce potentially long  
 452 range interactions. In this respect, it differs from most vertex-  
 453 based models (*e.g* [11, 26]) where turgor is an input of the  
 454 model. The numerical resolution required the development  
 455 of an original algorithm (see SI) implemented in an in-house  
 456 code.

457 **Numerical experiments: growth of primordia in the shoot apical**  
 458 **meristem (SAM).** The properties of this model cannot be  
 459 as thoroughly studied as those of the simpler models presented  
 460 above, first because of the numerical cost of the resolution,  
 461 but above all because it allows an infinite variety of geometries  
 462 and spatial distribution of its parameters. We present here a  
 463 numerical experiment that illustrates on the one hand how the  
 464 properties of the simple multidimensional and multicellular  
 465 submodels are combined in the generalized model; in turn the  
 466 study of these models helps us to anticipate the properties  
 467 of the generalized model. And on the other hand, we show  
 468 that this model is readily applicable to the study of systems  
 469 of biological interest.

470 Growth heterogeneities can be triggered by the local mod-  
 471 ulation of the mechanical properties of the cell walls [27]. In  
 472 SAMs, new organs are initiated by a local increase in growth  
 473 rate that leads to the appearance of small bumps. Measure-  
 474 ments show that physico-chemical properties of walls are mod-  
 475 ified so that mechanical anisotropy and elastic modulus are  
 476 decreased. In our 2D model, we can explore what effect a  
 477 local softening of the walls has on growth rate and turgor  
 478 heterogeneities; based on our previous analysis of the model  
 479 in simple configurations, we expect that the growth hetero-  
 480 geneities will be maximal for parameters such that the growth  
 481 is restricted by fluxes rather than wall synthesis (low  $\alpha^a$ ),  
 482 cell-cell conductivity is large, and the walls deformations are  
 483 just above the growth threshold, which can be enforced by a  
 484 low value of the osmotic pressure (yet large enough to ensure  
 485 growth). The set of parameters (REF) is chosen according  
 486 to these criteria; then we explore the effect of a higher  $\alpha^a$   
 487 ((ALPHA+) set) and lower cell-cell conductivity ((CC-) set)

497 that should both decrease the growth heterogeneities, and also  
498 test the effect of a lower osmotic pressure ((PM-) set) that  
499 should conversely increase the growth heterogeneity. See table  
500 1 in SI for the values of the parameters corresponding to these  
501 sets and SI for more precise explanations.

502 We build a mesh made primarily of hexagons (see Fig. 3a)  
503 and first let it grow with homogeneous parameters until the  
504 elastic regime ends and plastic growth occurs. Then we di-  
505 vide by two the elastic modulus of a small group of cells  
506 (marked with a white star in Fig. 3a) that will be referred to  
507 as “bump cells” thereafter. All the details of the computations  
508 are presented in SI. First, Fig. 3b shows that the multicellular  
509 system grows globally in the same way as the single hexagonal  
510 cell studied above; it diverges from the Lockhart predictions  
511 because the ratio  $A/V$  of the cells is not constant: the (AL-  
512 PHA+) simulations exhibit a very large initial growth rate  
513 that decreases only when the cells are so large that water  
514 fluxes become limiting. The (PM-) set leads to a roughly  
515 twice lower growth rate than (REF). The set (CC-) leads to  
516 the same dynamics at the tissue level as (REF), because the  
517 total influx of water is not affected by fluxes between cells in  
518 this setup.

519 Then we turn to the observation of heterogeneities: we focus  
520 on the differences between the bump region and the rest of the  
521 tissue. For all the parameters sets, Fig. 3c shows that turgor  
522 is in general lower in bump cells, but the gap varies depending  
523 on the parameters, as it has been predicted by the study of  
524 the two-cells model: compared to (REF), the heterogeneity  
525 in turgor is increased by a lower cell-cell conductivity (set  
526 CC-), and decreased by a larger value of  $\alpha^a$  (set ALPHA+).  
527 Decreasing the value of  $P^M$  (set PM-) does not alter much  
528 the turgor heterogeneity compared to (REF). The maps of  
529 turgor (Figs. 3e,g,i,k) confirm visually these observations.

530 Fig. 3d shows the time evolution of  $\dot{\gamma}/\dot{\gamma}^*$  where  $\dot{\gamma}^*$  is the  
531 relative growth rate predicted by the Lockhart model (see  
532 Eq. (6)); its value is  $2\% \text{ h}^{-1}$  for (REF), (CC-) and (ALPHA+),  
533 and  $0.5\% \text{ h}^{-1}$  for (PM-). In the considered time frame, the  
534 relative growth rate of bump cells is always higher except for  
535 (ALPHA+): after an initial fast increase where bump cells  
536 grow faster, the tendency is inversed at  $t \approx 20\text{h}$  because the  
537 bump cells have grown so much that fluxes become limiting. In  
538 the (REF) simulation, while the growth rate of non bump cells  
539 is almost constant and close to  $\dot{\gamma}^*$ , the growth rate of the bump  
540 cells is up to 6 times  $\dot{\gamma}^*$  at the beginning of the simulation and  
541 progressively decreases toward  $\dot{\gamma}^*$ . As a result of this large  
542 discrepancy, the bump region can be clearly distinguished from  
543 the rest of the tissue (Figs. 3e-f). In (CC-), the growth rate of  
544 the non bump cells is close to that of (REF), but the growth  
545 rate of the bump cells is much lower (Fig. 3d). As a result,  
546 the global shape remains convex and the bump is not clearly  
547 detached from the rest of the tissue (Figs. 3i-j). Note that  
548 (CC-) corresponds to a lower value of  $\alpha^s$  compared to (REF),  
549 which corresponded to a lower growth heterogeneity with the  
550 two-cells model studied above; this is also confirmed by the  
551 lower cell-cell fluxes towards the bump cells for (CC-), see  
552 the arrows in Figs. 3e,i. The (ALPHA+) simulation exhibits  
553 also a convex shape (Fig. 3k-l); it corresponds to a larger  
554 value of  $\alpha^a$  than (REF), and similarly to the two-cells model  
555 studied above, the growth rate heterogeneity is lower than  
556 (REF). Finally, the set (PM-) corresponds to an increase of  
557 the dimensionless parameter  $\rho$  (see Eq. (9)), and accordingly

558 to an increase in growth rate heterogeneity as can be seen  
559 with Fig. 3d. Consequently, the bump region can clearly  
560 distinguished from the rest of the tissue, even better than  
561 (REF) (Fig. 3g-h); moreover, the growth of the cells close to  
562 the bump seems to be inhibited by fluxes as explained in the  
563 two-cells model described above and further explored below.

564 **Flux-based lateral inhibition predicted by the model.** As we saw,  
565 cells that benefit from better mechanical conditions for growth  
566 (in the present case a lower elastic modulus) have a lower turgor  
567 than the other cells, and therefore attract water from them.  
568 Not only does it amplify their growth but it also inhibits  
569 the growth of their neighbours. Such a lateral inhibition  
570 mechanism is important for morphogenesis, as it allows very  
571 large growth rate heterogeneities and the appearance of well  
572 differentiated shapes (in the present case the appearance of a  
573 bump on the surface of the meristem). The efficiency of this  
574 mechanism varies depending on the position in the parameters  
575 space: for instance it is increased if the cell-cell conductivity  
576  $L^s$  (or equivalently  $\alpha^s$ ) is increased (see Fig. 4a-d); even  
577 the whole tissue can be inhibited. Inhibited cells can also  
578 relax the tension of their walls and decrease their volume (see  
579 Fig. 4a). To further explore and quantify the spatial range of  
580 this inhibition process, we extended our two-cells model (see  
581 SI for detailed equations) to a chain of  $2N + 1$  cells where  
582 the central cell has twice softer walls. We numerically solved  
583 the corresponding system of differential equations for the set  
584 (REF) and then for a large range of values of  $L^s$ . Fig. 4e shows  
585 that the number  $2N_i$  of inhibited cells scales with  $\sqrt{L^s}$ . We  
586 computed the prefactor  $c$  (such that  $N_i \approx c\sqrt{L^s}$ ) for values  
587 of  $(\alpha^a, P^M) \in [0.05, 0.35] \times [0.51, 0.85]$  (the interval for  $P^M$  is  
588 in MPa) and plotted its value in the  $(\alpha^a, P^M)$  space (Fig. 4f).  
589 This shows that the inhibition is favored by low values of  $\alpha^a$   
590 and  $P^M - P^Y$ .

## 593 Discussion

594 **A minimal model with a complex and rich behavior.** The model  
595 proposed in this article is a minimal multicellular and multidimensional extension of the Lockhart 1-D single cell model; it  
596 can be regarded as a conceptual tool to study the interplay  
597 between fluxes and wall mechanics in a multicellular tissue.  
598 Wall expansion is modeled with a visco-elasto-plastic rheological law, while fluxes derive from water potential gradients.  
599 These two contributions are integrated into the mechanical  
600 equilibrium and interact through the pressure term. Contrary  
601 to most previous approaches, turgor is not an input of the  
602 model but a variable that adjusts simultaneously to mechanical,  
603 hydraulic, and geometrical constraints. First of all, this  
604 leads to a physically consistent representation of turgor: for  
605 instance, the model predicts that cells with softer walls have  
606 a lower turgor. Moreover, this has deep implications at tissue  
607 level: in the previous example, lower turgor is associated with  
608 a faster growth which can be itself amplified by fluxes that  
609 follow decreasing pressure gradients.

610 Thanks to the simplicity of the model, the predicted behavior  
611 can be analyzed and interpreted with two submodels built  
612 from the Lockhart model: first, a 1-D multicellular submodel  
613 was build with two or more side-by-side cells; it was used to  
614 study the growth of competing cells with heterogeneous prop-  
615 erties. Key ingredients here are the wall synthesis threshold,  
616 the fact that fluxes and growth can relax turgor, and cell to  
617 cell fluxes that allow long range interactions. Second, in a  
618  
619  
620

621 1-D system, cells are considered essentially as cylinders and  
622 their surface-to-volume ratio is constant. We thus extended  
623 also the Lockhart model in two dimensions, where cells have  
624 more degree of freedom to change their shape. In particular  
625 their allometric surface-to-volume ratio may then vary. This  
626 new possibility induces additional complexity in the tissue  
627 development as the rate of growth of cell surfaces may become  
628 a limiting factor for growing cells.

629 **A potentially new type of lateral inhibition mechanism.** Depend-  
630 ing on mechanical and hydraulic parameters of tissue regions,  
631 the model exhibits different growth regimes corresponding to  
632 either uniform or differential growth. One unexpected conse-  
633 quence of such an hydraulic-mechanical coupling at the tissue  
634 level is the observation that in certain regions of the parameter  
635 space where cell-to-cell hydraulic exchanges are non-limiting,  
636 growing tissue may exert an inhibiting influence on the growth  
637 of neighboring regions. This may be interpreted as a lateral  
638 inhibition mechanism. It has for long been recognized that  
639 lateral inhibitory mechanisms play a key role in setting some  
640 morphogenetic patterns in procaryotes (e.g. [28]), animals (e.g.  
641 [29, 30]) or plants (e.g. [31, 32]). Lateral inhibition operates  
642 in these systems via chemical signals, such as delta-notch in  
643 animals or auxin in plants. Our model predicts the existence  
644 of a novel type of lateral inhibition mechanism based on the  
645 coupling between mechanics and water fluxes. Previous obser-  
646 vations of tissue growth suggest that such a phenomenon may  
647 occur in real tissues. In the shoot apical meristem for instance,  
648 detailed quantification of growth with cellular resolution indi-  
649 cates that the region surrounding primordia growth may have  
650 a negative growth rate [33], Figs. 2G and 3K. According to  
651 our model, this decrease of volume in boundary regions might  
652 be due to the primordium growth attracting locally most of  
653 the water supply and depriving lateral regions from water, and  
654 thus confornts the hypothesis of a new hydraulic-mechanical  
655 component of primordium lateral inhibition, beyond already  
656 identified auxin and cytokinin signals [34].  
657

658 **Model simplifications and further potential extensions.** Throug-  
659 hout the development of the model, we made several key choices  
660 concerning the abstraction of a multicellular plant tissue. First,  
661 our model was developed in 2-D for reasons of computational  
662 efficiency. In principle, it can be extended in 3-D, though at  
663 the expense of more complex formalism and implementation.  
664 Second, the current model considers that water transport is  
665 performed in the plant tissue through two conceptually differ-  
666 ent pathways ([1]). Water can first move within the apoplastic  
667 compartment between the cells and finally enter a cell. Water  
668 can also move locally from cell to cell. This movement includes  
669 itself conceptually both symplasmic movements (water circulates  
670 between cells through plasmodesmata without crossing  
671 membranes) and movements from cell to cell with intermedi-  
672 ate steps in the wall (water is for example exported locally  
673 out of the cell by water transporters like aquaporins into the  
674 wall and immediately re-imported by water transporters into  
675 neighboring cells). For sake of simplicity in this first analysis,  
676 we represented the apoplasm as a single abstract compartment  
677 able to exchange water with every cell. To analyze precisely  
678 the effect of water transporters and their genetic regulation or  
679 to assess the impact of wall resistance to water movement in  
680 the processes, explicit spatial representation of the apoplasm,  
681 of plasmodesmata and of membrane water transporters could  
682 be integrated into the model in the future.

683 Finally, we considered a simplified situation here by impos-  
684 ing constant cell osmolarity. Allowing osmolarity variations  
685 (for instance higher values in faster growing regions) may  
686 impact turgor distribution (e.g [35]). However, this should  
687 not affect the ability of the system to build up growth het-  
688 erogeneities. Similarly, we further simplified our model by  
689 keeping constant the apoplastic water potential. Relaxing  
690 this hypothesis would increase cell-cell water fluxes (via the  
691 apoplasm) and could also shift the model in the direction of  
692 the flux-limiting regime. This would therefore favor regimes  
693 where growth heterogeneities are amplified by fluxes.  
694

695 **ACKNOWLEDGMENTS.** This work has been carried out within  
696 the context of the project MecaFruit3D funded by the Agropolis  
697 foundation in Montpellier, France.  
698  
699  
700  
701  
702  
703  
704  
705  
706  
707  
708  
709  
710  
711  
712  
713  
714  
715  
716  
717  
718  
719  
720  
721  
722  
723  
724  
725  
726  
727  
728  
729  
730  
731  
732  
733  
734  
735  
736  
737  
738  
739  
740  
741  
742  
743  
744

745		807
746		808
747		809
748	1. Cosgrove D (1986) Biophysical control of plant cell growth. <i>Ann Rev Plant Physiol</i> 37:377–405.	810
749	2. Kutschera U (1991) Regulation of cell expansion. <i>The cytoskeletal basis of plant growth and form</i> pp. 85–99.	811
750	3. Cosgrove DJ (1993) Wall extensibility: its nature, measurement and relationship to plant cell growth. <i>New Phytol</i> 124(1):1–23.	812
751	4. Lockhart JA (1965) An analysis of irreversible plant cell elongation. <i>J Theor Biol</i> 8:264–275.	813
752	5. Coen E, Rolland-Lagan AG, Matthews M, Bangham JA, Prusinkiewicz P (2004) The genetics of geometry. <i>P Natl Acad Sci USA</i> 101(14):4728–4735.	814
753	6. Hamant O et al. (2008) Developmental Patterning by Mechanical Signals in Arabidopsis. <i>Science</i> 322(5908):1650–1655.	815
754	7. Alim K, Hamant O, Boudaoud A (2012) Regulatory role of cell division rules on tissue growth heterogeneity. <i>Front Plant Sci</i> 3:174.	816
755	8. Boudon F et al. (2015) A Computational Framework for 3D Mechanical Modeling of Plant Morphogenesis with Cellular Resolution. <i>PLOS Comput Biol</i> 11(1):e1003950–16.	817
756	9. Bidhendi AJ, Geitmann A (2016) Relating the mechanics of the primary plant cell wall to morphogenesis. <i>J Exp Bot</i> 67(2):449–461.	818
757	10. Dupuy L, Mackenzie JP, Haseloff JP (2006) <u>A biomechanical model for the study of plant morphogenesis: Coleochaete orbicularis, a 2D study species.</u>	819
758	11. Merks RMH, Guravage M, Inz e D, Beemster GTS (2011) VirtualLeaf: An Open-Source Framework for Cell-Based Modeling of Plant Tissue Growth and Development. <i>Plant Physiol</i> 155(2):656–666.	820
759	12. Dyson RJ et al. (2014) Mechanical modelling quantifies the functional importance of outer tissue layers during root elongation and bending. <i>New Phytol</i> 202:1212–1222.	821
760	13. Bassel GW et al. (2014) Mechanical constraints imposed by 3D cellular geometry and arrangement modulate growth patterns in the Arabidopsis embryo. <i>P Natl Acad Sci USA</i> 111(23):8685–8690.	822
761	14. Bozorg B, Krupinski P, Jönsson H (2016) A continuous growth model for plant tissue. <i>Phys Biol</i> 13(6):1–14.	823
762	15. Fozard JA, Lucas M, King JR, Jensen OE (2013) Vertex-element models for anisotropic growth of elongated plant organs. <i>Front Plant Sci</i> 4:233.	824
763	16. Peaucelle A et al. (2011) Pectin-induced changes in cell wall mechanics underlie organ initiation in Arabidopsis. <i>Curr Biol</i> 21(20):1720–1726.	825
764	17. Braybrook SA, Peaucelle A (2013) Mechano-Chemical Aspects of Organ Formation in Arabidopsis thaliana: The Relationship between Auxin and Pectin. <i>PLOS one</i> 8(3):e57813.	826
765	18. Sassi M et al. (2014) An Auxin-Mediated Shift toward Growth Isotropy Promotes Organ For-	827
766	mation at the Shoot Meristem in Arabidopsis. <i>Curr Biol</i> 24(19):2335–2342.	828
767	19. Jensen OE, Fozard JA (2015) Multiscale models in the biomechanics of plant growth. <i>Physiology</i> 30(2):159–166.	829
768	20. Cosgrove DJ (2018) Diffuse growth of plant cell walls. <i>Plant Physiol</i> 176:16–27.	830
769	21. Corson F et al. (2009) Turning a plant tissue into a living cell froth through isotropic growth. <i>P Natl Acad Sci USA</i> 106:8453–8458.	831
770	22. Long Y et al. (2018) Cellular heterogeneity in pressure and growth emerges from tissue topology and geometry. <i>bioRxiv</i> p. 334664.	832
771	23. Boyer JS (1988) Cell enlargement and growth-induced water potentials. <i>Plant Physiol</i> 73:311–316.	833
772	24. Ortega JKE (1985) Augmented growth equation for cell wall expansion. <i>Plant Physiol</i> 79:318–320.	834
773	25. Nobel PS (1970) <u>Introduction to biophysical plant physiology.</u> No. 581.1 N6.	835
774	26. Dupuy L, MacKenzie J, Rudge T, Haseloff J (2008) A system for modelling cell-cell interactions during plant morphogenesis. <i>Ann Bot</i> 101(8):1255–1265.	836
775	27. Kierzkowski D et al. (2012) Elastic domains regulate growth and organogenesis in the plant shoot apical meristem. <i>Science</i> 335(6072):1096–1099.	837
776	28. Yoon HS, Golden JW (1998) Heterocyst pattern formation controlled by a diffusible peptide. <i>Science</i> 282(5390):935–938.	838
777	29. Sternberg PW (1988) Lateral inhibition during vulval induction in <i>Caenorhabditis elegans</i> . <i>Nature</i> 335(6190):551–554.	839
778	30. Baker NE, Mlodzik M, Rubin GM (1990) Spacing differentiation in the developing <i>Drosophila</i> eye: a fibrinogen-related lateral inhibitor encoded by <i>scabrous</i> . <i>Science</i> 250(4986):1370–1377.	840
779	31. Reinhardt D et al. (2003) Regulation of phyllotaxis by polar auxin transport. <i>Nature</i> 426(6964):255–260.	841
780	32. Barbier de Reuille P et al. (2006) Computer simulations reveal properties of the cell-cell signaling network at the shoot apex in Arabidopsis. <i>P Natl Acad Sci USA</i> 103(5):1627–1632.	842
781	33. Kwiatkowska D, Dumais J (2003) Growth and morphogenesis at the vegetative shoot apex of <i>Anagallis arvensis</i> L. <i>J Exp Bot</i> 54(387):1585–1595.	843
782	34. Besnard F et al. (2014) Cytokinin signalling inhibitory fields provide robustness to phyllotaxis. <i>Nature</i> 505(7483):417–421.	844
783	35. Ruan YL, Llewellyn DJ, Furbank RT (2001) The control of single-celled cotton fiber elongation by developmentally reversible gating of plasmodesmata and coordinated expression of sucrose and K <sup>+</sup> transporters and expansin. <i>Plant Cell</i> 13(1):47–60.	845
784		846
785		847
786		848
787		849
788		850
789		851
790		852
791		853
792		854
793		855
794		856
795		857
796		858
797		859
798		860
799		861
800		862
801		863
802		864
803		865
804		866
805		867
806		868



869  
870  
871  
872  
873  
874  
875  
876  
877  
878  
879  
880  
881  
882  
883  
884  
885  
886  
887  
888  
889  
890  
891  
892  
893  
894  
895  
896  
897  
898  
899  
900  
901  
902  
903  
904  
905  
906  
907  
908  
909  
910  
911  
912  
913  
914  
915  
916  
917  
918  
919  
920  
921  
922  
923  
924  
925  
926  
927  
928  
929  
930

931  
932  
933  
934  
935  
936  
937  
938  
939  
940  
941  
942  
943  
944  
945  
946  
947  
948  
949  
950  
951  
952  
953  
954  
955  
956  
957  
958  
959  
960  
961  
962  
963  
964  
965  
966  
967  
968  
969  
970  
971  
972  
973  
974  
975  
976  
977  
978  
979  
980  
981  
982  
983  
984  
985  
986  
987  
988  
989  
990  
991  
992

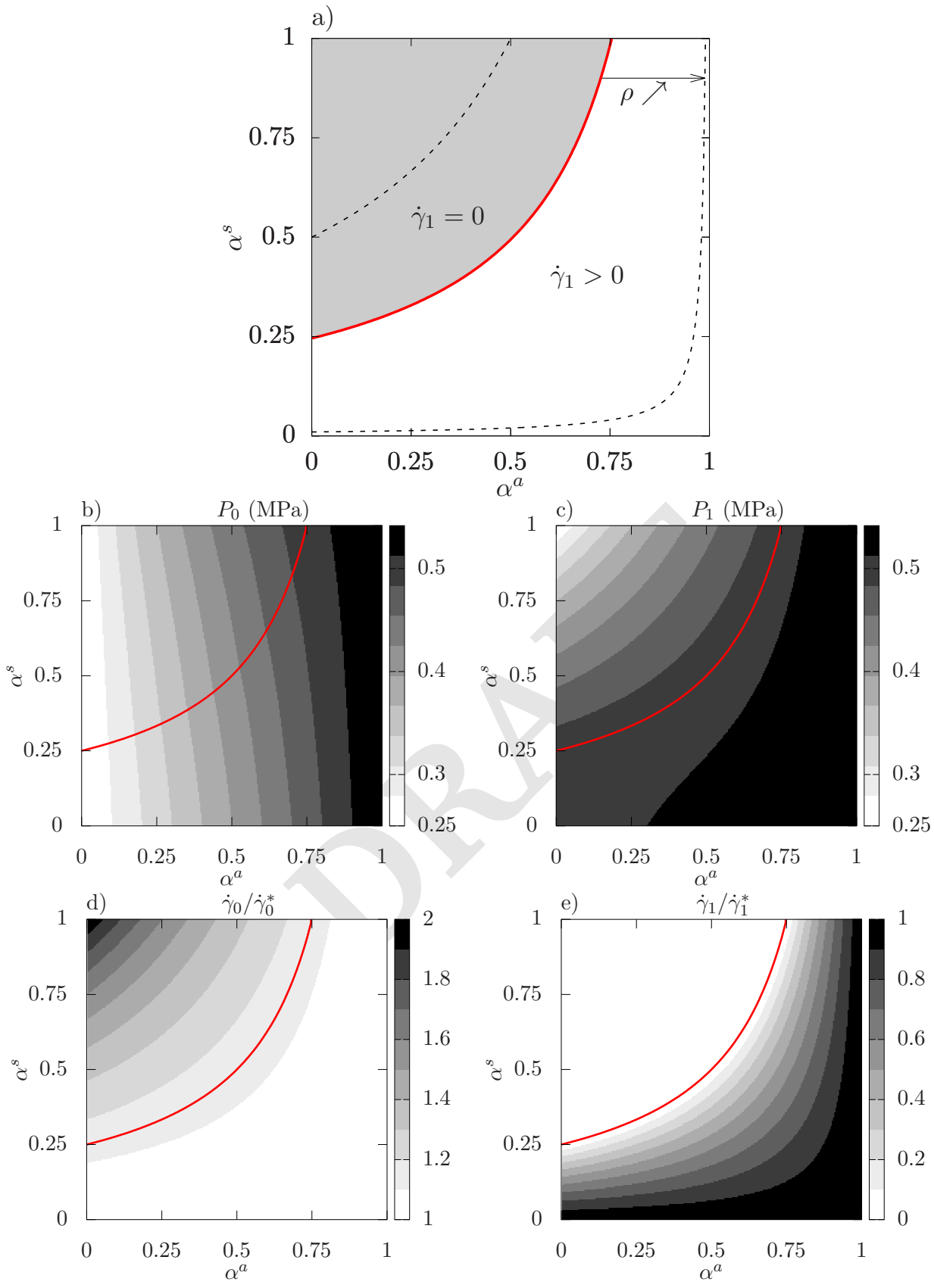


**Fig. 2.** Analytical resolution of the two cells model, properties of the solution in the parameters space  $\alpha^a \times \alpha^s$ ; **a)** delimitation of the two zones  $\dot{\gamma}_1 = 0$  and  $\dot{\gamma}_1 > 0$ : the red thick solid line  $\alpha^s(\alpha^a) = \frac{1-\rho}{1-\alpha^a}$  corresponds to  $\rho = 0.75$ . The two black thin dashed lines correspond to the values  $\rho = 0.5$  and  $0.99$ . **b-c)** Turgors  $P_0$  and  $P_1$  for  $\rho = 0.75$ . **d-e)** relative growth rates  $\dot{\gamma}_i/\dot{\gamma}_i^*$  for  $\rho = 0.75$ .

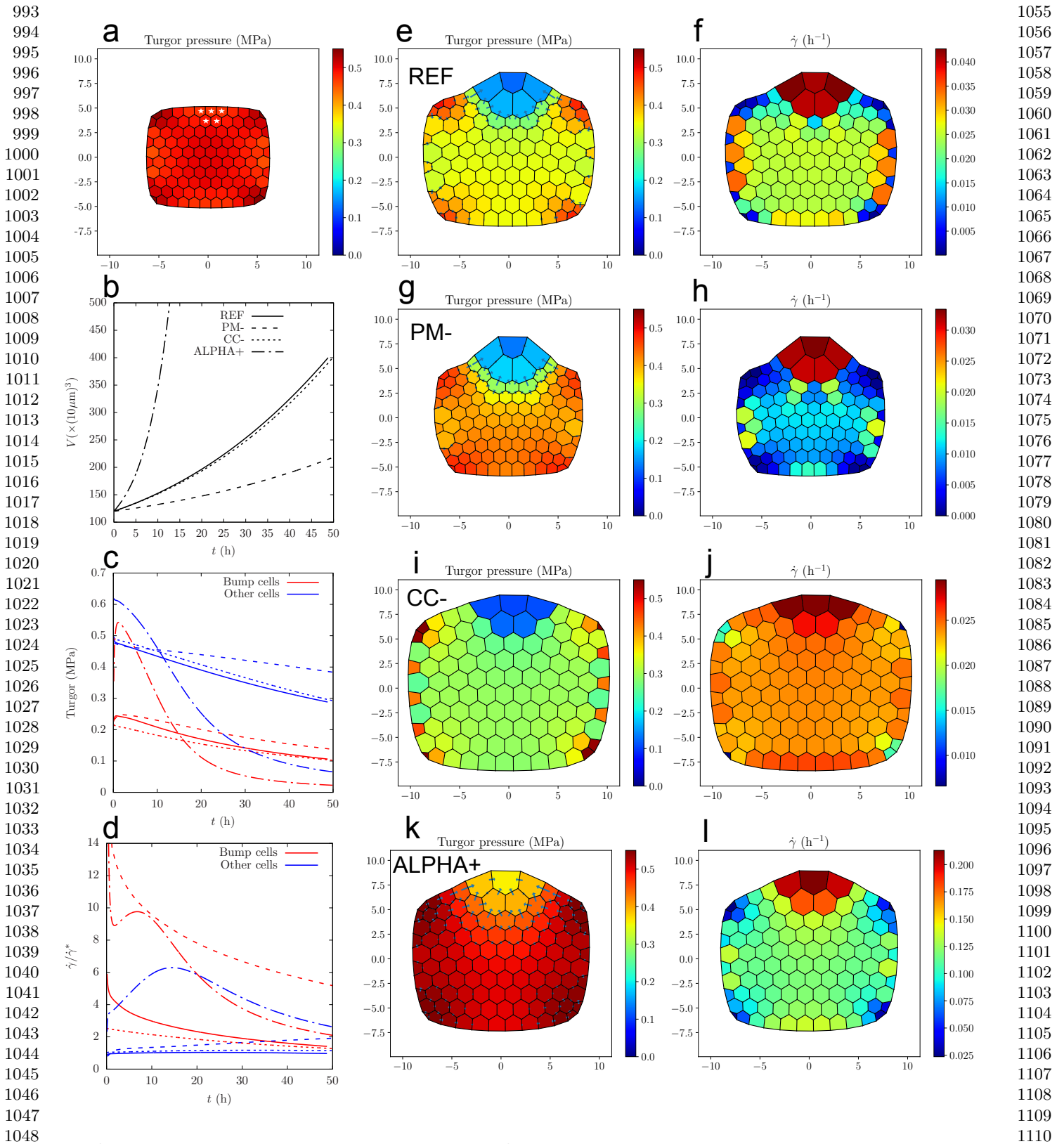


**Fig. 3.** Growth of tissue with heterogeneous mechanical parameters, see table 1 in SI. **(a)** Initial state for (REF): walls are under tension because of turgor and have reached their yield deformation. At  $t = 0$ , the walls of the cells marked with a white star are softened (the elastic modulus is divided by two). **(b)** Time evolution of the total volume. The dashtype of the lines distinguishes the parameters sets; the same dashtype convention is used in **(c)** and **(d)**. **(c)** Time evolution of turgor pressure of bump cells (red) and other cells (blue). **(d)** Time evolution of relative growth rate of bump cells (red) and other cells (blue). **(e-l)** Turgor and relative growth rate maps of parameters sets (REF) (**(e-f)**), (PM-) (**(g-h)**), (CC-) (**(i-j)**), and (ALPHA+) (**(k-l)**), at the time when the volume of the bump cells has increased by a factor 5:  $t = 51\text{h}$  for (REF),  $t = 33\text{h}$  for (PM-),  $t = 80\text{h}$  for (CC-),  $t = 14.8\text{h}$  for (ALPHA+). The arrows represent the intensity and direction of cell-cell water fluxes; the scale for arrows is the same for (REF), (PM-) and (CC-) and close to 4 times higher for (ALPHA+).

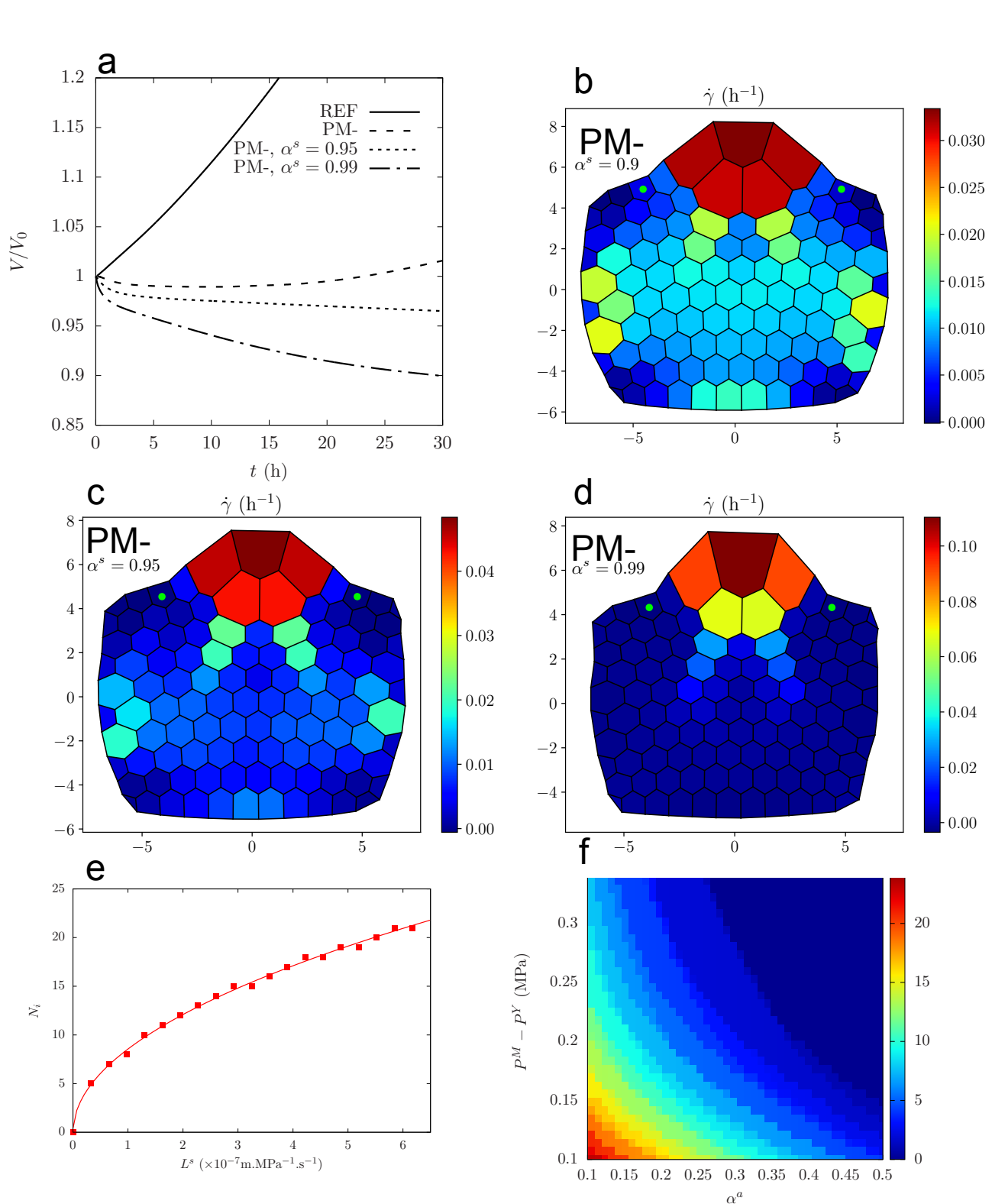


**Fig. 4.** Evidence of lateral inhibition: left: **a**) time evolution of the volume of two cells on the boundary of the bump (marked with a green dot on the maps **b, c, d**) with the sets of parameters (REF), (PM-), (PM-) with  $\alpha^s = 0.95$ , (PM-) with  $\alpha^s = 0.99$ .  $V_0$  is the volume of the cells at  $t = 0$ . **b, c, d**) maps of relative growth rate at  $t = 33\text{h}$  for (PM-),  $t = 20\text{h}$  for (PM-) and  $\alpha^s = 0.95$ ,  $t = 10\text{h}$  for (PM-) and  $\alpha^s = 0.99$ . **e-f**) Results for a chain of  $2N + 1$  cells with  $N = 50$ , where the central cell has twice softer walls; **e**) number  $N_i$  of cells that are inhibited on each side of the central cell, for different values of  $L^s$ ; the line is a fit with a square root function, in the form  $c\sqrt{L^s}$ . **f**) Values of the prefactor  $c$  in the space  $(\alpha^a, P^M)$ .